Cambridge Centre for Computational Chemical Engineering

University of Cambridge

Department of Chemical Engineering

Preprint ISSN 1473 – 4273

Two-stage Fuel Direct Injection in a Diesel Fuelled HCCI Engine

Haiyun Su, Sebastian Mosbach, Markus Kraft [1], Amit Bhave [2], Sanghoon Kook, Choongsik Bae [3],

Draft of November 5, 2007

[1] Department of Chemical Engineering
University of Cambridge
Pembroke Street
Cambridge CB2 3RA
UK
E-Mail: markus_kraft@cheng.cam.ac.uk

[2] Reaction Engineering Solutions Ltd.
61 Canterbury Street
Cambridge CB4 3QG
UK
E-Mail: amitbhave@resolutionsltd.com

[3] Department of Mechanical Engineering
Korea Advanced Institute of Science and Technology
373-1 Kusong-Dong, Yusong-Gu, Taejon
305-701
Korea
Email: csbae@kaist.ac.kr

Preprint No. 46

c4e

Key words and phrases: HCCI, wall impingement, cetane number, spray

Edited by
Cambridge Centre for Computational Chemical Engineering
Department of Chemical Engineering
University of Cambridge
Cambridge CB2 3RA
United Kingdom.

Fax: + 44 (0)1223 334796
E-Mail: c4e@cheng.cam.ac.uk
World Wide Web: http://www.cheng.cam.ac.uk/c4e/

Abstract

Two-stage fuel direct injection (DI) has the potential to expand the operating region and control the auto-ignition timing in a Diesel fuelled homogeneous charge compression ignition (HCCI) engine. In this work, to investigate dual-injection HCCI combustion, a stochastic reactor model, based on a probability density function (PDF) approach, is utilized. A new wall-impingement sub-model is incorporated into the stochastic spray model for direct injection. The model is then validated against measurements of combustion parameters and emissions carried out on a four stroke HCCI engine. The initial results of our numerical simulation reveal that the two-stage injection is capable of triggering the charge ignition on account of locally rich fuel parcels under certain operating conditions, and consequently extending the HCCI operating range. Furthermore, both simulated and experimental results on the effect of second injection timing on combustion indicate that there exists an optimal second injection timing to gain maximum engine output work for a given fuel split ratio.

Contents

1 Introduction

Development of advanced combustion technologies such as Homogeneous Charge Compression Ignition (HCCI) is an important facet in the drive towards advancing high efficiency, low emissions capable engine technologies. However in addition to its intrinsic benefits in terms of near-zero emissions of NO_x and particulate matter, HCCI engine operation faces technical challenges such as difficulty in robust control of auto-ignition timing, narrow operating range, and mixture formation [1]. In particular, for challenges related to HCCI engine operation, various strategies for mixture formation namely, port fuel injection (PFI), early DI, late DI and multiple injection have been investigated to help overcome the aforementioned obstacles [2, 3, 4, 5]. Various control techniques such as variable compression ratio, heating intake air and/or fuel, external exhaust gas recirculation (EGR) and variable injection angle have been implemented to help realise HCCI combustion in internal combustion (IC) engines [1]. In practice, only a near-homogeneous charge of air and Diesel is possible before the onset of compression ignition, and this operation mode is known by its variant name -premixed charge compression ignition (PCCI).

To tackle the aforesaid issues of PCCI or HCCI combustion, two-stage direct injection of Diesel has been demonstrated as a promising solution by various researchers [4, 6, 7]. In that, an early direct injection event (main injection) was utilised to create a premixed charge and was then followed by a second injection event close to top dead centre (TDC). The second injection event acted as a charge stratification agent and as an ignition promoter of the PCCI combustion. Additionally, through the variation of injection timing the combustion characteristics such as the auto-ignition timing were also controlled. Furthermore, realisation of non-luminous combustion near TDC (virtually zero soot) and reduction of NO_x emissions were also reported. However, some issues still stay unresolved with HCCI. First of all, the early DI is carried out when the in-cylinder pressure is near-atmospheric. Thus the penetration of fuel spray is much greater than in conventional CIDI combustion, and can result in wall impingement. The liquid fuel deposited on the wall and the fuel-rich zones close to the wall contribute to increased emissions and losses in engine performance. Additionally, the inherent characteristics of Diesel fuel make its evaporation difficult and aggravate the mixture formation problem.

In parallel to the experimental research, a variety of computational modelling approaches have been applied to gain insight into Diesel fuelled PCCI operation. For instance, controlling the mixing of air and fuel during the time interval between end of injection and start of combustion for Diesel fuelled early DI (36 crank angle degree (CAD) before top dead centre (BTDC)) HCCI operation has also been studied using Reynolds Averaged Navier Stokes (RANS) as well as coarse grid Large Eddy Simulation (LES) based models [8, 9]. Kim and Reitz studied the effect of early DI timing (51 to 15 CAD BTDC) on combustion characteristics in a light duty Diesel engine operating in premixed compression ignition mode, using KIVA CFD code (with sub-models for spray-wall interactions) along with a reduced n-heptane chemistry [10]. An optimum injection timing corresponding to the impingement of the spray at the edge of the piston crown was shown to enhance the mixing of air and

fuel effectively with the help of squish flow and the droplet splash behaviour. The same modelling approach was utilised to simulate a single cylinder engine with split injection. In particular, perfect homogeneity resulting from the first injection was assumed, and the second injection timing was optimised to after TDC to show the reduction in diffusion combustion temperature and NO_x emissions [11]. Recently, another CFD-based approach involving KIVA and a multi-zone combustion model has been implemented by Flowers et al. to simulate PCCI engine operation [12]. Again, a mapping technique to group the CFD grid cells into finite zones for kinetics calculations and re-mapping the information back from zone to cell was used to reduce the computational expense. However, to simulate a non-homogeneous PCCI combustion case, fuel spray and mixing dynamics were approximated by imposing the fuel-air distribution. Elsewhere, a CFD code including the description of the effect of cavitation on the nozzle discharge coefficient, spray-wall interaction, auto-ignition and a 3-zone coherent flame model for combustion has also been used to simulate a dual mode Diesel engine operation termed narrow angle direct injection (NADI) with split injection [13].

Two system level modelling approaches based on a 1-D engine cycle code (to account for gas exchange) integrated with a multi-zone combustion model [14] and with a CFD driven external model [15] have been applied to simulate PCCI engine operation modes. While a simplistic air-fuel distribution was specified in the multi-zone approach, two numerical grids of different resolution (refined grid for spray dynamics and air-fuel mixing, and mapping on a coarse grid for kinetics) were adopted in the CFD driven approach.

With the aim of developing a system level simulation tool capable of providing sufficiently reliable predictions for combustion parameters as well as emissions, and for carrying out systematic parametric sensitivity studies within reasonable computational times, the probability density function (PDF) based stochastic reactor model (SRM) is used to simulate a dual DI Diesel fuelled PCCI engine. This closed volume model can be easily incorporated in an engine cycle code without major modifications. The SRM approach includes detailed kinetics description and accounts for inhomogeneities in composition and temperature due to turbulent mixing, convective heat transfer and direct injection [16, 17, 18]. Furthermore, as the fuel spray impingement and the resulting phenomena such as rebound, spread and splash have a strong influence on combustion characteristics in PCCI combustion, the SRM was extended to account for such fluid-wall interactions. The turbulent mixing is modelled using the Euclidean Minimum Spanning Tree (EMST) concept [19].

This paper is structured as follows. In the next section, the numerical model is presented and the spray sub-models and their implementation in the SRM framework are explained. This is followed by the description of the geometry and operating conditions of the single cylinder engine used in this investigation. In the next section, results of the detailed numerical study are presented. In that the model calibration for a motored engine cycle and the influence of wall impingement and other model parameters on the model calculations are discussed. Furthermore, model predictions such as in-cylinder pressure, auto-ignition timing as well as CO, HC and NO_x emissions are compared with the values obtained from measurements. The effect of

dual injection on PCCI combustion is explained on the basis of a model-predicted composition PDF for fuel. The detailed explanation of the experimental results can be found in a previous publication [7].

2 SRM for DI HCCI and Sub-models

The SRM has been successfully employed in previous work [16, 17, 18]. A brief outline of the main features of the model has been included in the appendix. The sub-models describing the spray and the wall impingement are explained in the following subsections. The output of the model consists of (distributions of) the species mass fractions Y_j, temperature T and liquid fuel mass m_l, combined into a vector $\psi = (Y_1, ..., Y_s, T, m_l)$ for notational convenience, where S denotes the number of chemical species. The source terms generating the time evolution of the PDF represent the various processes taken into account by the model, i.e. chemical kinetics, turbulent mixing, piston movement, convective heat transfer, stochastic spray and fuel evaporation.

In this study, the SRM is extended to account for fuel-wall interactions. The sub-models for wall impingement, fuel evaporation and crevices will be discussed here in detail. In the numerical model, chemical kinetics of Diesel fuel combustion is represented in terms of elementary chemical reactions of n-heptane combustion consisting of 157 chemical species and 1551 reactions. To represent Diesel fuel's physical characteristics in the direct injection model, n-dodecane is considered as a surrogate since its molecular weight is close to the average molecular weight of Diesel. In addition, the fuel amount is modified by a factor of 0.86 based on the ratio of the combustion heats of Diesel and n-heptane (The heat value of Diesel is set at 45.5 kJ/kg and a value of 52.7 kJ/kg is used for n-heptane).

2.1 Wall impingement

Wall impingement is quite common in DI spark ignition (SI), PFI SI engine and small-size CIDI engines. For dry wall, the droplet impingement regimes can be categorised as sticking, reflecting and sliding depending on the Weber number of the incident drop [20]. Bai and Gosman [21], Santan and Rutland [22] proposed a splash regime for wetted wall. Since it is assumed that wall impingement occurs in the wetting region in this work, Bai and Gosman's model was employed.

Wall impingement takes place when the tip of the fuel spray reaches the cylinder liner or the surface of the piston head. Under the simplifying assumption that the shape of the volume penetrated by the liquid fuel is a cone, it can be determined by means of elementary geometry whether or not any liquid fuel has reached the wall. The impingement criterion is then fulfilled if at least one of the following holds:

$$S(t) \cdot \sin(\theta/2) > \text{Bore}/2 \tag{1}$$

or

$$S(t) \cdot \cos(\theta/2) > \frac{4V(t)}{\pi \mathrm{Bore}^2}, \tag{2}$$

where θ denotes the full cone angle, and $V(t)$ the current cylinder volume. The spray tip penetration $S(t)$ is calculated by Hiroyasu's [23] empirical equations:

$$S(t) = \begin{cases} 0.39 \left(\frac{2\Delta p}{\rho_l}\right)^{1/2} t & t < t_{\mathrm{break}} \\ 2.95 \left(\frac{\Delta p}{\rho_g}\right)^{1/4} (d_n t)^{1/2} & t > t_{\mathrm{break}} \end{cases}, \tag{3}$$

where

$$t_{\mathrm{break}} = \frac{28.65 \rho_l d_n}{(\rho_g \Delta p)^{1/2}}, \tag{4}$$

Δp is the pressure drop across the nozzle, ρ_l and ρ_g are the fuel liquid and gas densities respectively, d_n is the nozzle diameter, and t is time since the start of injection (see also [24]).

In order to model what happens to the fuel droplets after they have hit the wall, the transition criteria of impingement regimes proposed by Bai and Gosman [21] are employed here:

$$\begin{aligned} &\text{Stick :} && \mathrm{We}_n \leq 2 \\ &\text{Rebound :} && 2 < \mathrm{We}_n \leq 20 \\ &\text{Spread :} && 20 < \mathrm{We}_n \leq \mathrm{We}_c \\ &\text{Splash :} && \mathrm{We}_c < \mathrm{We}_n \end{aligned} \tag{5}$$

where We_n denotes the normal Weber number ($\mathrm{We}_n = \rho_l d_d (v \cdot \sin(\theta/2))^2/\sigma$), $\mathrm{We}_c = 1320\mathrm{La}^{-0.1826}$, La the Laplace number, and σ the surface tension. The velocity of the droplets is derived by

$$v = \frac{\mathrm{d}S(t)}{\mathrm{d}t} = \begin{cases} 0.39 \left(\frac{2\Delta p}{\rho_l}\right)^{1/2} & t < t_{\mathrm{break}} \\ 1.475 d_n \left(\frac{\Delta p}{\rho_g}\right)^{1/4} (d_n t)^{-0.5} & t > t_{\mathrm{break}} \end{cases}. \tag{6}$$

When fuel splash occurs, it rebounds from the wall and breaks up. The ratio of total secondary droplet's mass m_s and the incident drop mass m_i is given by

$$r_m = \frac{m_s}{m_i} = (0.2 + 0.9 \cdot \Omega_{\mathcal{U}(0,1)}) \tag{7}$$

where $\Omega_{\mathcal{U}(0,1)}$ denotes a uniformly distributed random number between 0 and 1 [21]. For simplification, $\Omega_{\mathcal{U}(0,1)}$ is replaced by a mean value of 0.5 in the present work. Furthermore, in order to account for multiple droplet interactions during the impingement and fuel trapped in the crevice or at the corner of the squish area during the compression stroke, r_m is corrected as $0.65 f_{\mathrm{eff}}$.

The calculation of the secondary droplet size is discussed below.

2.2 Spray and impingement breakup

The Sauter mean diameter SMD of fuel droplets after first breakup is calculated as

$$\text{SMD} = A_H \Delta P^{-0.135} \rho_g^{0.121} V_l^{0.131}, \tag{8}$$

where $A_H = 23.9$ for hole nozzles, ΔP is the mean pressure drop across the nozzle, ρ_g is the air density, and V_l is the volume of fuel delivered per injection pulse [23]. If the impingement occurs before the primary breakup, it is assumed that SMD $= d_n$.

After the impingement, the mean volumetric diameter d_m is given as

$$d_m = \left(\frac{r_m}{30 \frac{We_n}{We_c} - 1} \right)^{1/3} d_i,$$

where d_i is the incident droplet diameter. It is assumed that the size distribution of the secondary droplets is given by the Nukiyama-Tanasawa function [25]:

$$f(d) = \frac{2}{3} \frac{d^2}{d_m^3} \exp\left[- \left(\frac{d}{d_m} \right)^{3/2} \right]. \tag{9}$$

A droplet population distributed according to this function possesses a Sauter mean diameter of $d_{32} \approx 2.16 d_m$.

In a previous paper [17], a simplistic spray model was developed, which does not take into account spatial information. For charge stratification, It is assumed that the inflowing fuel is distributed at a constant rate such that no fluid parcel receives fuel at more than one instant in time. More quantitatively, there are a fraction α of all parcels will receive fuel, where α is defined as

$$\alpha = \frac{\text{Mass of charge receiving liquid fuel}}{\text{Total mass of charge}}. \tag{10}$$

In a time step Δt, the mass of cylinder charge that is to be endowed with fuel droplets is given by $\alpha M_{\text{tot}} \Delta t / (\text{injection duration})$, where M_{tot} denotes total mass of the charge. Physically, larger α corresponds to more evenly spread fuel, e.g. greater cone angle. Contrariwise, smaller α implies stronger charge stratification. α is formulated such that it is independent of the number of particles.

2.3 Evaporation sub-model

The mass flow rate of evaporation $\dot{m}_d$ is calculated as:

$$\dot{m}_d = -\pi^{2/3} (\frac{6}{\rho_l})^{1/3} \cdot \rho_g D_g \text{Sh}_0 \ln(1 + B_M) m_d^{1/3}, \tag{11}$$

where d_d is the droplet diameter, D_g is the vapour/air binary diffusion coefficient, Sh_0 is the Sherwood number and B_M is the Spalding mass transfer number. Then the droplet diameter is updated by

$$d_d = \left(\frac{6 m_d}{\rho_l \pi} \right)^{1/3}. \tag{12}$$

The Spalding mass transfer number is given by

$$B_M = \frac{Y_{fs} - Y_\infty}{1 - Y_{fs}}, \tag{13}$$

where Y_{fs} is fuel mass fraction at the droplet surface, Y_∞ is fuel mass fraction of surrounding gas. In addition an evaporation parameter $\zeta = \langle \mathrm{Sh}_0 \rangle / 2$ was used, where $\langle \mathrm{Sh}_0 \rangle$ represents mean Sherwood number over the evaporation duration.

That leads to:

$$\dot{m}_d = -2\zeta\pi^{2/3}(\frac{6}{\rho_l})^{1/3} \cdot \rho_g D_g \ln(1 + B_M) m_d^{1/3}, \tag{14}$$

It is assumed that there is no temperature gradient inside the droplet. Thus, the droplet temperature can be updated by

$$\frac{\mathrm{d}T_d}{\mathrm{d}t} = \frac{1}{m_d c_{p_l}}(\dot{Q}_d - \dot{m}_d H_v), \tag{15}$$

where c_{p_l} is the fuel heat capacity and H_V denotes the enthalpy of vaporization.

The heat transfer rate $\dot{Q}_d$ is calculated as:

$$\dot{Q}_d = -\dot{m}_d \cdot c_{pf} \frac{T - T_d}{B_T}, \tag{16}$$

where c_{pf} is the specific heat capacity of vapour, T is the temperature of surrounding gas, T_d is the droplet temperature and B_T is the Spalding heat transfer number. As the ratio B_T/B_M was found approximately between 1.05 and 1.2 [26], $B_T = 1.1 B_M$ was chosen in this study.

The PDF transport equation is extended to include the time evolution of m_l by setting

$$G_{S+2} = -2\zeta\pi^{2/3}(\frac{6}{\rho_l})^{1/3} \cdot \rho_g D_g \ln(1 + B_M) m_d^{1/3} N_d^{2/3}, \tag{17}$$

where $m_l = N_d \times m_d$ and N_d is the number of droplets in the population.

2.4 Crevice sub-model

The engine cylinder chamber is split into two parts -the crevice and the bulk. The charge temperature in the crevice is assumed to be equal to the wall temperature. Applying the ideal gas law in the bulk as well in the crevice yields

$$\begin{aligned} p &= \frac{mRT}{VM} \\ p_{\mathrm{cr}} &= \frac{m_{\mathrm{cr}} R T_{\mathrm{cr}}}{V_{\mathrm{cr}} M_{\mathrm{cr}}} \end{aligned} \tag{18}$$

where $p, p_{\mathrm{cr}}, m, m_{\mathrm{cr}}, M, M_{\mathrm{cr}}, T, T_{\mathrm{cr}}, V, V_{\mathrm{cr}}$ stand for pressure, mass, molecular weight, temperature and volume of the bulk and the crevice respectively. R denotes gas constant.

If $p > p_{\mathrm{cr}}$, charge flows from the bulk into the crevice. The mass transferred in a time step Δt is denoted by Δm. The pressure of the chamber is in balance, leading to

$$\frac{m-\Delta m}{M}\frac{RT}{V} = (\frac{m_{\mathrm{cr}}}{M_{\mathrm{cr}}} + \frac{\Delta m}{M})\frac{RT_{\mathrm{cr}}}{V_{\mathrm{cr}}}. \tag{19}$$

Then Δm can be calculated as:

$$\Delta m = \frac{m\frac{T}{V} - \frac{M}{M_{\mathrm{cr}}}m_{\mathrm{cr}}\frac{T_{\mathrm{cr}}}{V_{\mathrm{cr}}}}{\frac{T}{V} + \frac{T_{\mathrm{cr}}}{V_{\mathrm{cr}}}}. \tag{20}$$

When $p < p_{\mathrm{cr}}$, charge flows out from the crevice, leading to

$$\frac{m}{M}\frac{RT}{V} + \frac{\Delta m}{M_{\mathrm{cr}}}\frac{RT_{\mathrm{cr}}}{V} = \frac{m_{\mathrm{cr}}-\Delta m}{M_{\mathrm{cr}}}\frac{RT_{\mathrm{cr}}}{V_{\mathrm{cr}}} \tag{21}$$

Then Δm can be calculated as:

$$\Delta m = \frac{m_{\mathrm{cr}}\frac{T_{\mathrm{cr}}}{V_{\mathrm{cr}}} - m\frac{M_{\mathrm{cr}}}{M}\frac{T}{V}}{\frac{T_{\mathrm{cr}}}{V} + \frac{T_{\mathrm{cr}}}{V_{\mathrm{cr}}}}. \tag{22}$$

2.5 Spray/Impingement/Evaporation Algorithm

It is assumed that all droplets allocated to a stochastic particle have the same temperature and size. Thus,

$$m_l^{(i)} = N_d^{(i)} \times m_d^{(i)}, i = 1, \ldots, N_{\mathrm{par}}.$$

1. Pick particles randomly and no particle which has been chosen previously is picked again. Assign to each of the chosen particles a value of $m_l^{(i)}$ proportional to the statistical weight such that the total injected mass $\sum m_l^{(i)}$ per time step Δt equals $\dot{m}_{\mathrm{fuel}}\Delta t$, i.e.
$$m_l^{(i)} = \frac{W^{(i)}}{\sum W^{(j)}}\dot{m}_{\mathrm{fuel}}\Delta t,$$
where the sum ranges over the indices of the chosen particles.

2. Initialise $d_d^{(i)} = d_n$ and calculate the droplet numbers according to
$$N_{\mathrm{d}}^{(i)} = \frac{6m_l^{(i)}}{\pi\rho_l {d_d^{(i)}}^3} \qquad \forall i \in \{1, \ldots, N_{\mathrm{par}}\}. \tag{23}$$

3. Obtain spray penetration $S(t)$.

4. *Wall impingement:* Calculate v, We_c, We_n, d_m, when spray tip reaches the wall or piston surface. Set $m_l^{(i)} \mapsto \tilde{m}_l^{(i)}$, $d_d^{(i)} = d_{32}$, where

$$\begin{aligned}\tilde{m}_l^{(i)} &= m_l^{(i)} \times r_m \\ d_{32} &= 2.16 \times d_m \\ r_m &= (0.2 + 0.9\Omega_{u(0,1)}) f_{eff}\end{aligned}$$

5. Update the number of droplets according to (23).

6. *Evaporation:* Update the liquid fuel mass and temperature of all particles, i.e. for each $i \in \{1, \ldots, N_{\text{par}}\}$ set $m_l^{(i)} \mapsto \tilde{m}_l^{(i)}$, $T_l^{(i)} \mapsto \tilde{T}_l^{(i)}$, where

$$\begin{aligned}\tilde{m}_l^{(i)} &= m_l^{(i)} + \dot{m}_l^{(i)} \Delta t \\ \tilde{T}_l^{(i)} &= T_l^{(i)} + \tfrac{1}{m_l^{(i)} c_{p_l}} (\dot{Q}_l^{(i)} + \dot{m}_l^{(i)} H_v) \Delta t \\ \dot{m}_l^{(i)} &= -\pi \cdot 2\zeta d_d^{(i)} \rho_g D_g \ln(1 + B_M) N_d^{(i)} \\ \dot{Q}_l^{(i)} &= -\dot{m}_l^{(i)} \cdot c_{p_f} \tfrac{T^{(i)} - \tilde{T}_l^{(i)}}{1.1 B_M}\end{aligned}$$

   or set $m_l^{(i)}$ (and $N_{\text{d}}^{(i)}$) to zero if $\tilde{m}_l^{(i)}$ is non-positive.

7. Update the droplet diameter for all particles according to

$$d_d^{(i)} = \sqrt[3]{\frac{6 m_l^{(i)}}{\pi \rho_l N_{\text{d}}^{(i)}}} \qquad \forall i \in \{1, \ldots, N_{\text{par}}\}.$$

8. Calculate the enthalpy, $[W^{(i)} H^{(i)} - \dot{Q}_l^{(i)} \times \Delta t + (m_l^{(i)} - \tilde{m}_l^{(i)}) H_f^{(i)}]$ for all $i \in \{1, \ldots, N_{\text{par}}\}$.

9. Update the statistical weights according to

$$W^{(i)} \mapsto W^{(i)} + m_l^{(i)} - \tilde{m}_l^{(i)} =: \tilde{W}^{(i)}$$

   for all $i \in \{1, \ldots, N_{\text{par}}\}$.

10. Update the (gaseous) species mass fractions according to

$$\begin{aligned}Y_j^{(i)} &\mapsto Y_j^{(i)} \frac{W^{(i)}}{\tilde{W}^{(i)}} =: \tilde{Y}_j^{(i)} \quad \forall j \neq \text{fuel} \\ Y_{\text{fuel}}^{(i)} &\mapsto 1 - \sum_{j=1, j \neq \text{fuel}}^{S} \tilde{Y}_j^{(i)}\end{aligned}$$

    and update the temperature from enthalpy (Step 8) for all $i \in \{1, \ldots, N_{\text{par}}\}$, where 'fuel' denotes the indices of all fuel species.

3 Experimental Set-up

A single-cylinder optical Diesel engine running in PCCI (Premixed Charge Compression Ignition) mode was considered in this study. A common-rail fuel injection system was used to control the fuel injection pressure, injected quantity and injection timings. The engine description and the operating parameters are given in Table 1.

Table 1: *Engine specifications and operating parameters.*

Description	**Value**	**Units**
Displaced Volume	498	cm^3
Bore	83	mm
Stroke	92	mm
Connection rod	147	mm
Speed	800	RPM
Fuel	Diesel	–
Compression ratio	18.9	–
EVO/EVC	126.4/368.4 ATDC	CAD
IVO/IVC	$351/-135$ ATDC	CAD
Injection pressure	1200	bar
Injection timing of the single injection	$200, 150, 100$ BTDC	CAD
Second injection timing	$-20, -10, 0$ ATDC	CAD
Injection split ratio	$11.5 : 0, 10 : 1.5$	–
Fuel quantity	11.5	mm^3
Injection angle	100	^{o}
Intake air temperature	433	K
Intake air pressure	1	bar

The engine was operated at 800 RPM under motored and fired conditions. The coolant temperature was mainatined at 353 K and the Diesel fuel temperature was controlled at 313 K. These operating conditions represent an idling condition of a CIDI engine. The engine was equipped with a 5-hole nozzle injector with an injection angle of 100^o. Compression ratio was set high at 18.9 in order to promote auto-ignition at the idling condition. A more detailed description of the engine geometry and operating conditions is given elsewhere [7]. This engine was modelled using the SRM and the results of the model validation and parametric sensitivity tests are discussed in the next section.

4 Results and Discussion

Initially the SRM was calibrated to simulate the motored engine operation.

4.1 Motored-cycle calibration

In the experimental setup, the bore diameter equals 83 mm and the piston diameter is 81.3 mm. Thus, there is a gap of 0.85 mm between the piston and the cylinder wall. This geometrical feature can result in a strong blow-by and heat loss to the cylinder wall, and thus reduce the peak pressure dramatically. In addition, the compression ratio 18.9 was measured in a commercial engine and not in the optical research engine used for this work. Therefore, it is necessary to calibrate the model to account for these effects.

In this paper, a crevice model is implemented to account for the influence caused by the gap. The crevice ratio, which is defined as the ratio of the crevice volume to the cylinder clearance volume, is used to represent the size of the crevice. Figure 1 demonstrates the comparison of simulated and experimental values for in-cylinder pressure profile as a function of CAD. It can be observed from Figure 1 that the in-cylinder peak pressure is over-predicted when the effect of the crevice is not taken into account (crevice ratio=0%). The in-cylinder pressure profiles obtained by setting the crevice ratio to 4% and 8% are also displayed in Figure 1. An alternative approach of decreasing the compression ratio has also been adopted by other researchers to account for the gap [27]. In our test it was observed that by varying the effective compression ratio in the model, the pressure profile did not match the experimental data as well as when the crevice model was used. Furthermore, physical properties (temperature and concentration) and combustion characteristics are different for the charge in the crevice and the bulk. Therefore, incorporation of the crevice sub-model in the simulation was the preferred option for the present work.

4.2 Evaporation parameter validation

Two virtual cases are simulated to validate the model, including a n-dodecane droplet with diameter of 50 μm and a Diesel droplet with diameter of 25 μm. The droplet (50 μm in diameter) temperature and droplet diameter profiles with the elongation of evaporation time under typical HCCI combustion conditions are plotted in Figure 2. During the simulation, the surrounding gas pressure is 10 bar and the temperature is 1500 K. The initial temperature of liquid fuel is 300 K.

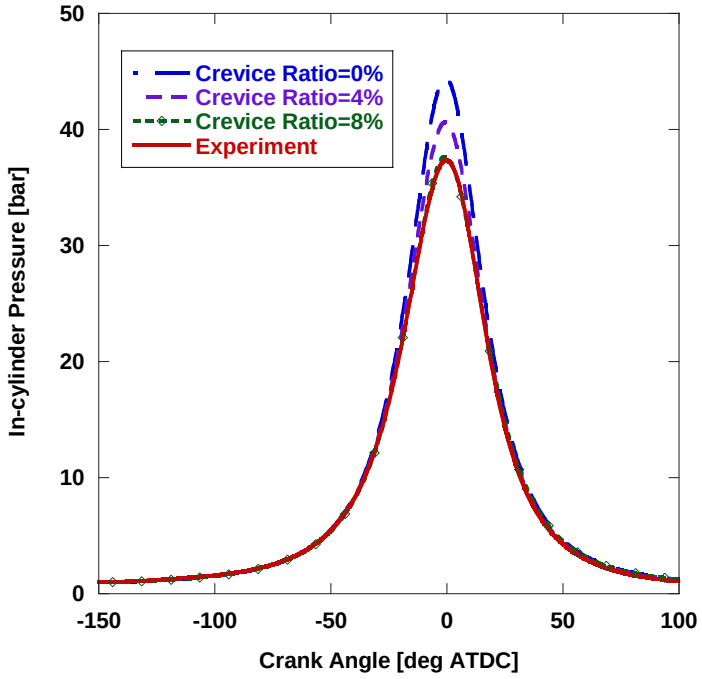

Figure 1: *Comparison of mean in-cylinder pressure as a function of CAD under motored condition (Measurements and simulation results with varying crevice ratios and compression ratio set to 18.9).*

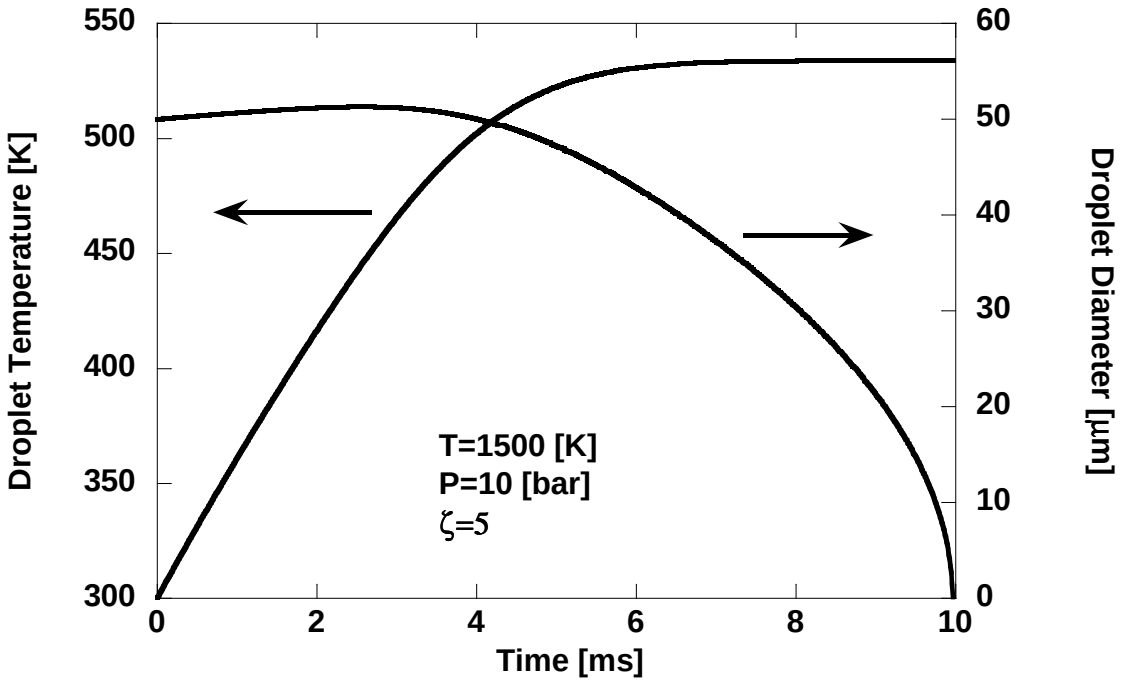

Figure 2: *The temperature and droplet diameter profiles of a n-dodecane droplet with the elongation of evaporation time under typical HCCI combustion conditons. Droplet diameter: 50 micron, Surrounding gas pressure: 10 bar, surrounding gas temperature: 1500 K. Evaporation parameter ζ = 5.*

Figure 2 shows that the evaporation time is 10ms, which is very close to the data published elsewhere [26]. However, the droplet temperature predicted by our model increases a bit slower. This is probably due to the assumption that there is no temperature gradient inside the droplet, whereas in Abramzon and Sirignano's work, the temperature simulated is the surface temperature of the droplet.

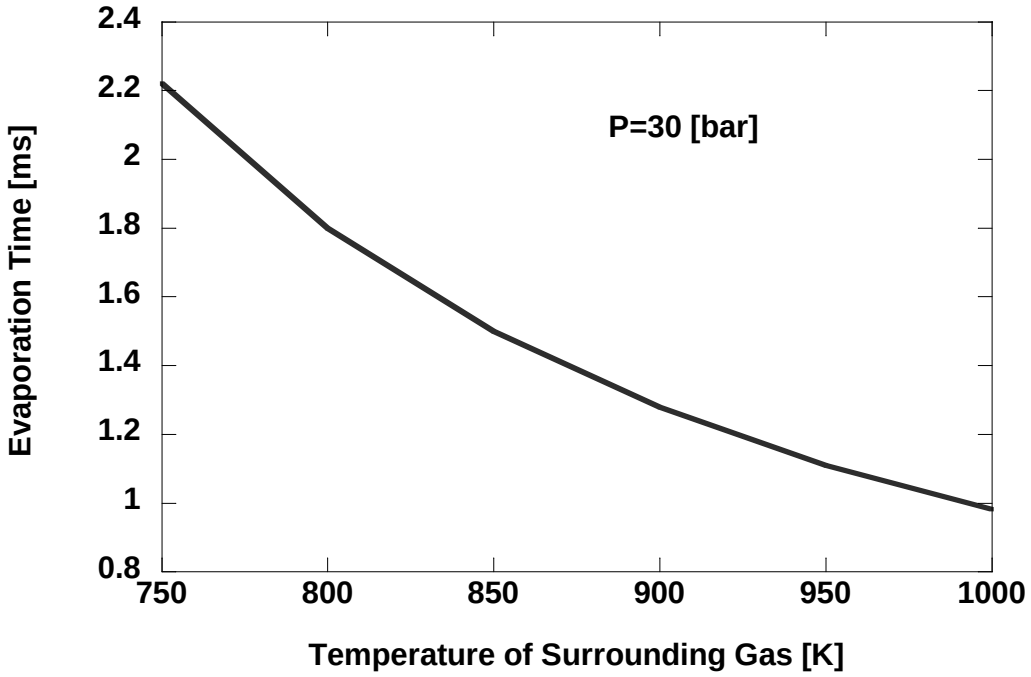

Figure 3: *Effect of the temperature of the surrounding gas on the evaporation time of a 25 μm Diesel droplet. Surrounding gas pressure: 30 bar. Evaporation parameter ζ = 5.*

Fig. 3 demonstrates that under typical Diesel conditions (Temperature = 1000 K), a droplet 25 μm in diameter evaporates in about 1 ms. This prediction is consistent with the value published in the literature [24].

In the following study, since the engine speed is low and the mean turbulent velocity is low as well, the evaporation parameter is chosen as 3. Crevice ratio is 8% and the mixing time is set to 10 ms except during the injection period when it is set to 5 ms.

4.3 Influence of wall impingement

When Diesel fuelled HCCI combustion is achieved through early direct injection, the issue of over-penetration of fuel arises, i.e., fuel impinging on the cylinder wall. Under such circumstances, a significant part of liquid fuel is lost. Some unburnt fuel is lost via the exhaust and some is trapped in the cylinder crevice and deposited on the piston surface. In this section, the influence of multiple droplet interactions during the wall impingement is studied.

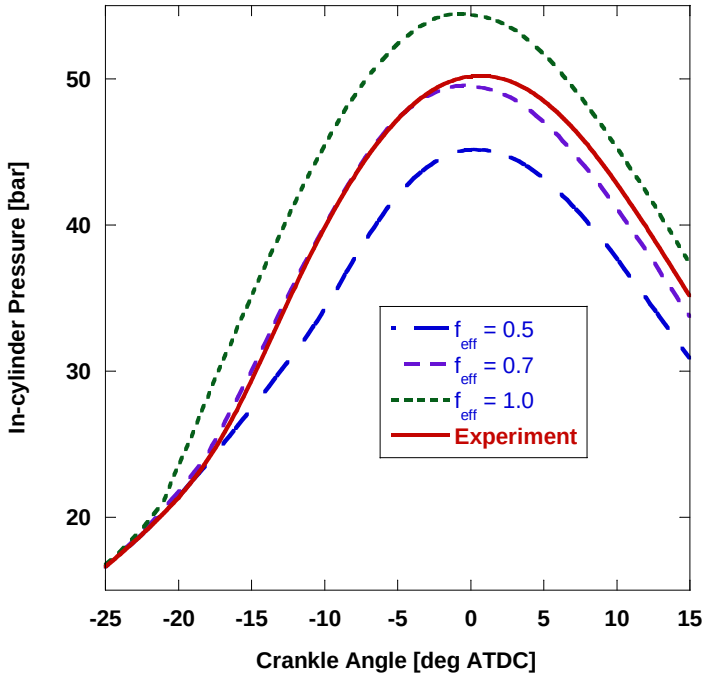

Figure 4: *Influence of wall impingement effectiveness on experimental and simulated in-cylinder pressure at SOI=-100 ATDC.*

Fig. 4 shows that, with the injection timing at -100 ATDC, when f_{eff} (Eqn. 7)equals 0.7, the simulated in-cylinder pressure profile matches the experimental data reasonably well. This also means that about half of the fuel is lost due to wall-wetting.

4.4 Single injection

For single injection, cases with different injection timing, namely, -200, -150 and -100 CAD ATDC, have been studied. The in-cylinder pressure and heat release rate (HRR) of single injection, with injection timing set to -200 and -100 CAD ATDC respectively, are shown in Figure 5.

The simulated pressure profiles and the start of two heat release rate peaks for both cases match the experimental data reasonably well. The comparison of measurements and simulated results for CO, NO_x and HC emissions are summarised in Table 2.

From Table 2, it can be observed that earlier the injection timing, the smaller the value of the parameter α. This is on account of the fuel spray that penetrates into a larger combustion chamber volume with advancement of injection timing. For example, f_{eff} was set to 0.55 for -200 and -150 CAD cases, but it was changed to 0.7 for -100 CAD. For injection timing at -100 ATDC, the air density is higher, which could cause atomization of more fuel droplets and lowering of droplet velocity as compared to the cases with injection timings -200 and -150 CAD ATDC.

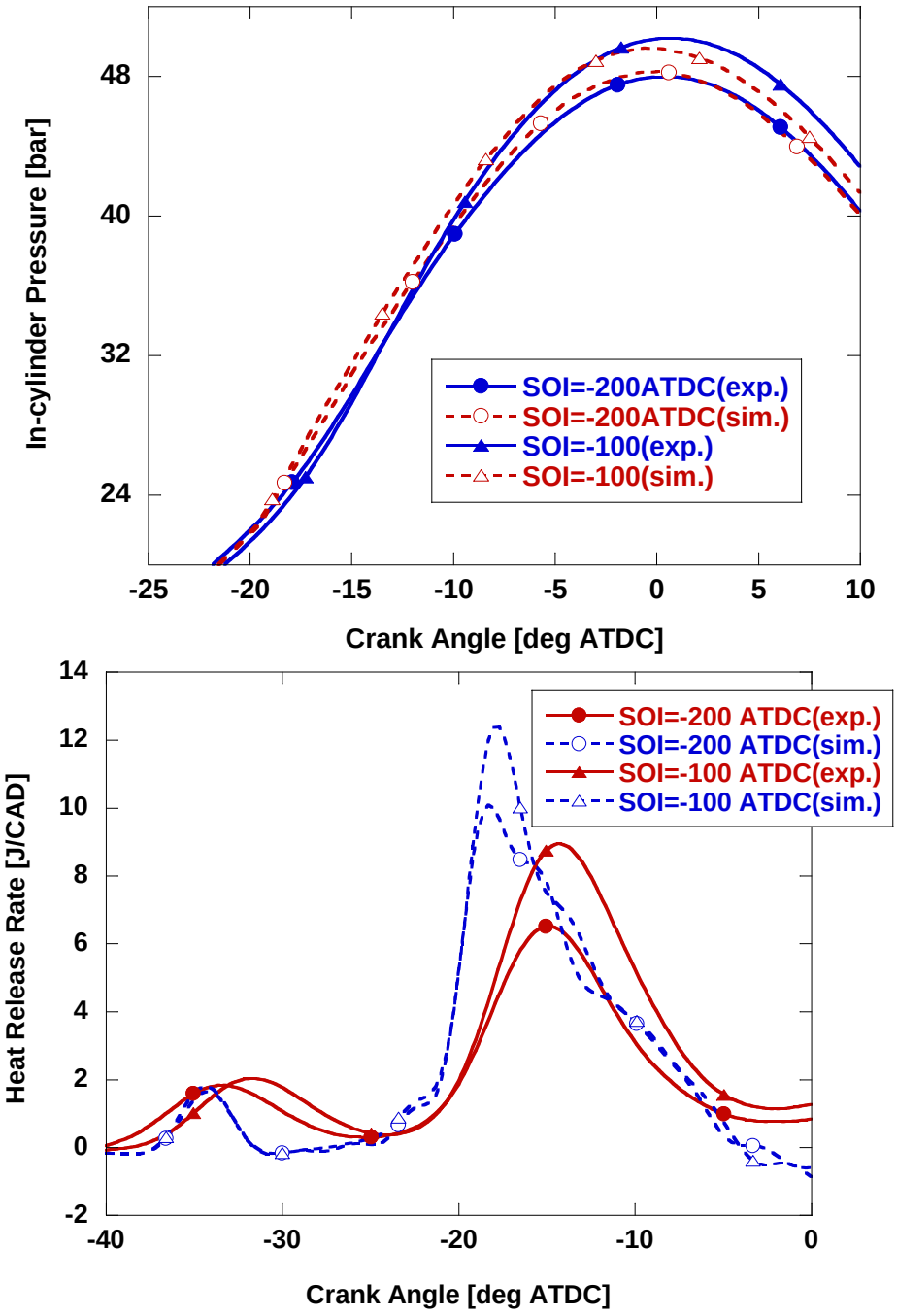

Figure 5: *Experimental and simulated in-cylinder pressure profiles as a function of crank angle for single injection at injection timing -200 and -100 ATDC.*

Table 2: *Comparison of simulated and experimental emissions*

	Experimental Data			Simulated Data				
Injection Timing	NO_x	HC	CO	NO_x	HC	CO	f_{eff}	α
-200	6.4645	3025.4	5190.8	5.9	4749.1	1514.5	0.55	0.011
-150	6.132	3425.6	5391.5	6.8	4569.7	1659.3	0.55	0.0254
-100	5.852	3545.1	4207.9	6.2	4832.3	1684.3	0.7	0.0973

HC emissions shown in Table 2 are higher than the experimental data whereas CO is under-predicted as compared to the measurements. The model does not take into account the chemical reactions close to the liquid film on the wall, which might explain the under-prediction of CO emissions.

4.5 Two-stage injection

To study the influence of the second injection timing, the main injection timing is set to -200 ATDC to achieve a near-homogeneous charge, the second injection timing is fixed at -20 ATDC to enhance engine output power, and the fuel amount split ratio of 10:1.5 is employed to take advantage of early-injection while auto-ignition is promoted. In addition, spray parameter α is set to 0.12 in the simulation.

Table 3: *Experimental and simulated and experimental emissions for single and dual injection*

	NO_x	HC	CO
Single injection (exp.)	6.5	3025	5191
Single injection (sim.)	5.3	4737	2224
Dual injection (exp.)	289.8	3601	4311
Dual injection (sim.)	337.2	3818	1778

The observed in-cylinder pressure enhancement and heat release rate of the dual injection case in comparison to single injection during combustion is depicted in Figure 6. The start of main heat release was slightly under-predicted by SRM. This is due to the fact that the SRM does not include a diffusion model, which is crucial to the injection timing close to TDC. Experimental and simulated emissions for single and dual injection are displayed in 3. Similar to the results in Table 2, the simulated CO emissions are consistently lower than experimental values for both single and

dual injection cases. Table 3 also demonstrates that NO_x emission by dual injection engine is higher than those by single injection. This is mainly because the local fuel rich area formed during second injection leads to locally higher temperatures.

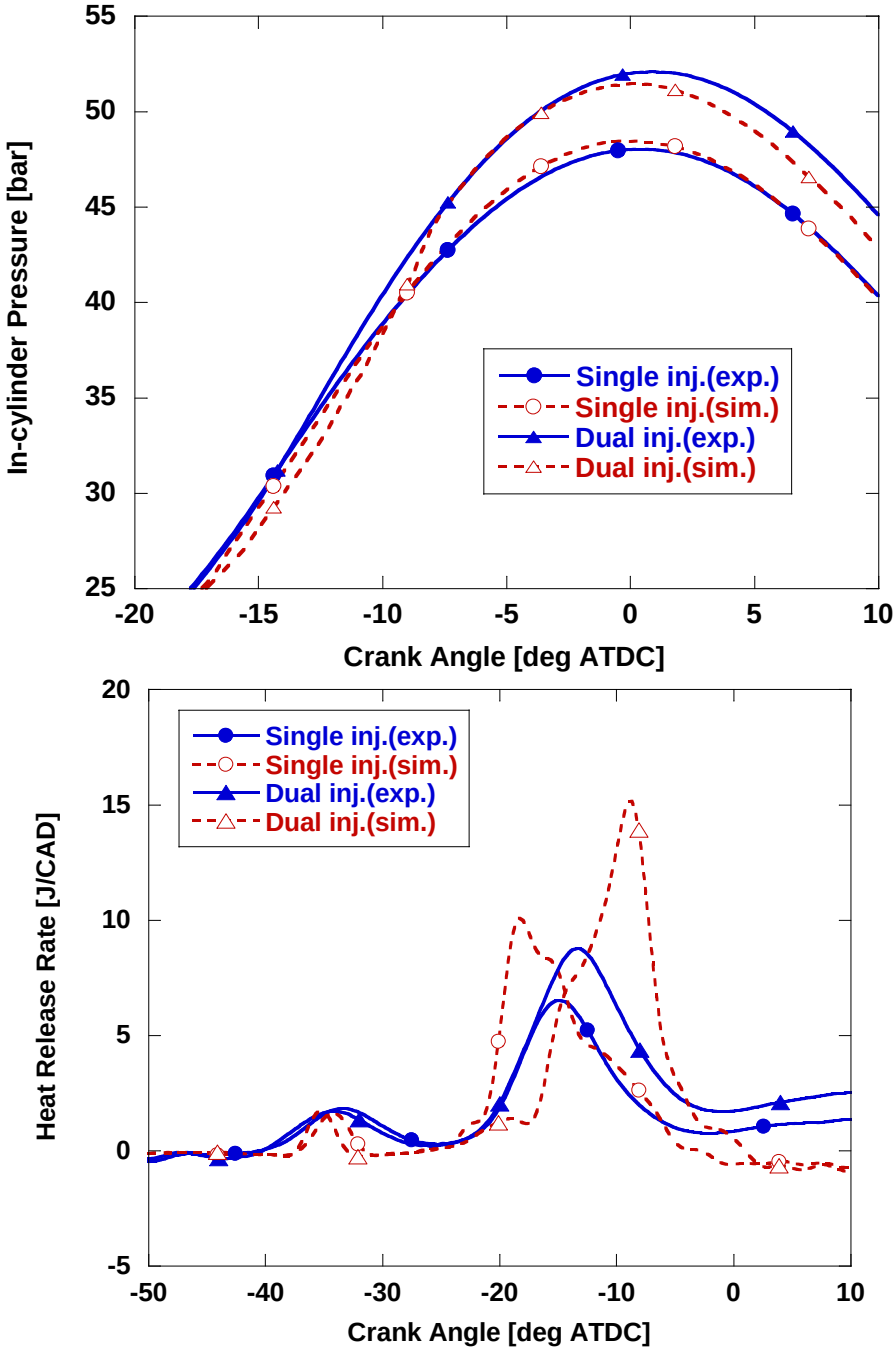

Figure 6: *Experimental and simulated in-cylinder pressure profiles as a function of CAD for single and dual injection.*

This explanation is further supported by the results shown in Figure 7, in which one can observe that a more stratified charge, i.e. more locally rich fuel parcels, is

formed as a result of second injection. On account of the temperature and composition conditions of these relatively rich regions being conducive for auto-ignition, combustion initiates in these regions. Later, these regions act as promoters for auto-ignition of the surrounding lean air-fuel mixture formed following the first injection event. Moreover, HCCI operating regime can be extended.

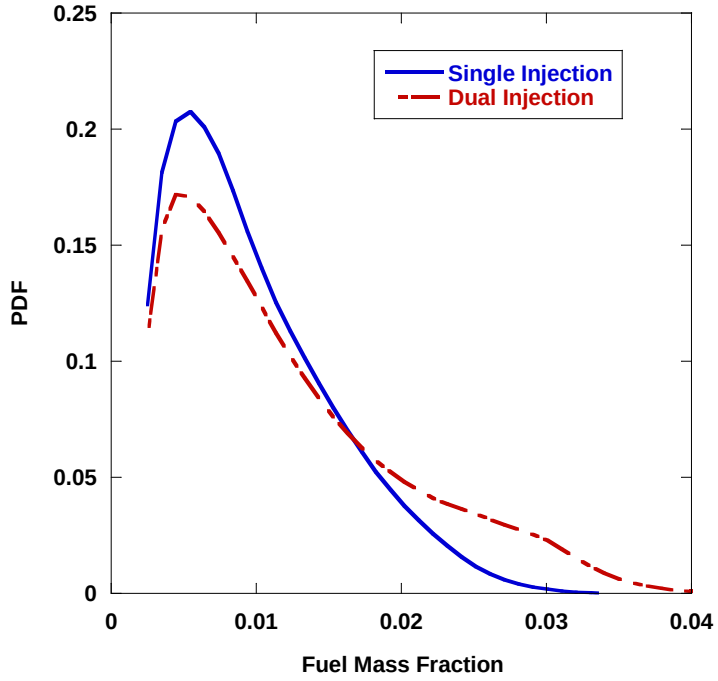

Figure 7: *Fuel mass fraction PDF at TDC: Single and dual injection cases.*

4.6 Effect of second injection timing

To further study the effect of second injection timing on combustion characteristics of PCCI operation, the in-cylinder peak pressure and heat release rate profiles were calculated with varying second injection timing while the other operating conditions used were the same as before. For second injection timing at -10 and 0 ATDC α was set to 0.15 and 0.25 respectively. The simulation results were verified by comparing them with experimental data.

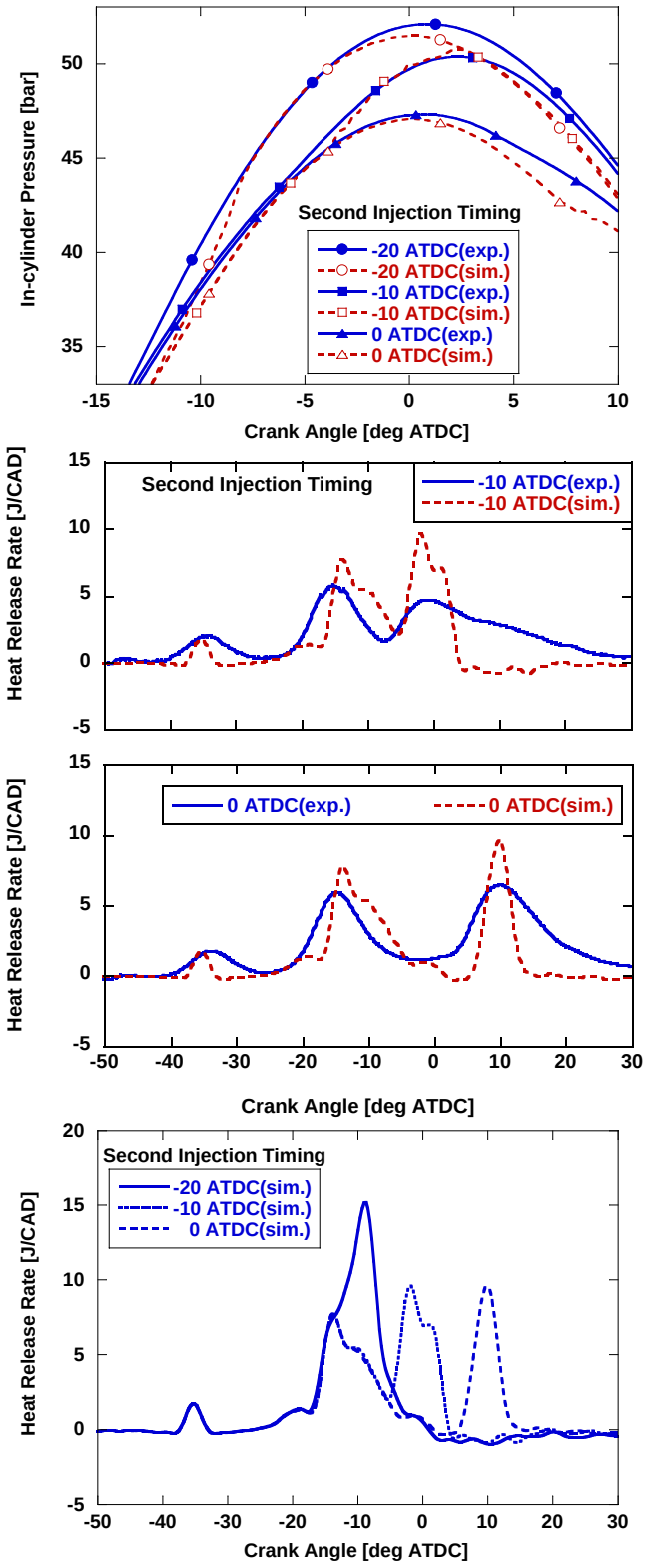

Figure 8: *Effect of second injection timing on experimental and simulated in-cylinder pressure and heat release rate profiles for dual injection.*

Figure 8 shows that the simulated results agree with the experimental data reasonably well. Both simulation and experiments demonstrate that the in-cylinder peak pressure consistently dropped when the second injection timing was varied from -20 to 0 ATDC. This can be explained by the fact that, for injection timing -10 and 0 ATDC, the fuel does not have sufficient time to evaporate and to start combustion after the second heat release peak. Our prediction is further confirmed by the heat release rate profiles for varying second injection timings, as a third heat release peak was observed when the second injection timings were set to -10 and 0 ATDC. The presence of the third heat release peak is caused by the combustion due to the second injection. Therefore, for the given fuel split ratio there exists an optimal second injection timing close to the start of main heat release, since the increase of the in-cylinder temperature can facilitate fuel evaporation and combustion.

5 Conclusions

In this work, a stochastic reactor model, based on a probability density function (PDF) approach has been developed further in order to simulate a Diesel-fuelled dual-injection premixed charge compression ignition (PCCI) combustion. In particular, the spray sub-model has been extended to incorporate wall impingement.

The evaporation sub-model was validated against data published in the literature. It was found that, under representative Diesel-fuelled HCCI engine conditions, when the evaporation parameter ζ equaled 5, the evaporation time of a Diesel droplet with a diameter of 25 m was consistent with the value in the literature.

Simulation results indicated that multiple droplet interaction due to wall impingement caused more fuel losses. The sub-model was validated against experimental results for combustion parameters and emissions. For the early direct injection, it was observed that the factor accounting for multiple droplet impingement increased from 0.55 to 0.77, when the injection timing was varied from -200 to -100 CAD ATDC.

The initial results of our numerical simulation revealed that the two-stage injection was capable of triggering the charge ignition owing to the local rich fuel parcels formed by the second injection. This resulted in longer combustion duration, and consequently extended the HCCI operating range. In addition, further study on the the effect of second injection timing showed that for a given fuel split ratio there was an optimal second injection timing to achieve the maximum work output from the engine.

Simulated results in this study have also demonstrated that fuel loss was quite serious in the cases with early direct injection. Potential methods such as variation in number and diameter of injector holes, reduction of injection angle and optimization of the injection timing in order to reduce and even avoid the fuel loss have been proposed in the literature.

References

[1] F. Zhao, T. Asmus, D. N. Assanis, J. E. Dec, J. A. Eng, and P. M. Najt. *Homogeneous Charge Compression Ignition HCCI Engines: Key research and Development Issues*. SAE PT-94, 2003.

[2] T. W. Ryan III and T. J. Callahan. Homogeneous charge compression ignition of diesel fuel. *SAE paper, No. 961160*, 1996.

[3] H. Akagawa, T. Miyamoto, A. Harada, S. Sasaki, N. Shimazaki, T. Hashizume, and K. Tsujimura. Approaches to solve problems of the premixed lean diesel combustion. *SAE paper, No. 1999-01-0183*, 1999.

[4] R. Hasegawa and H. Yanagihara. HCCI combustion in DI diesel engine. *SAE paper, No. 2003-01-0745*, 2003.

[5] S. Kimura, O. Aoki, H. Ogawa, S. Muranaka, and Y. Enomoto. New combustion concept for ultra-clean and high-efficiency small DI diesel engines. *SAE paper, No. 1999-01-3681*, 1999.

[6] H. Ogawa, N. Miyamoto, A. Sakai, and K. Akao. Combustion in a two-stage PCCI engine with lower distillation temperature fuels. *SAE paper, No. 2004-01-1914*, 2004.

[7] S. Kook and C. Bae. Combustion control using two-stage diesel fuel injection in a single-cylinder PCCI engine. *SAE paper, No. 2004-01-0938*, 2004.

[8] R. Jhavar and C. J. Rutland. Effects of mixing on early injection diesel combustion. *SAE paper, No. 2005-01-0154*, 2005.

[9] R. Jhavar and C. J. Rutland. Using large eddy simulations to study mixing effects in early injection diesel engine combustion. *SAE paper, No. 2006-01-0871*, 2006.

[10] M. Kim, R. D. Reitz, and S. C. Kong. Modeling early injection processes in hsdi diesel engines. *SAE paper, No. 2006-01-0056*, 2006.

[11] Y. Sun and R. D. Reitz. Modeling diesel engine NOx and soot reduction with optimised two-stage combustion. *SAE paper, No. 2006-01-0027*, 2006.

[12] D. Flowers, S. M. Aceves, and A. Babajimopoulos. Effect of charge non-uniformity on heat release and emissions in PCCI engine combustion. *SAE paper, No. 2006-01-1363*, 2006.

[13] B. S. Revielle, C. Habchi, A. P. Kleemann, and V. Knop. Potential of narrow angle direct injection diesel engines for clean combustion: 3D CFD analysis. *SAE paper, No. 2006-01-1365*, 2006.

[14] K. Narayanaswamy and C. J. Rutland. Cycle simulation diesel HCCI modelling studies and control. *SAE paper, No. 2004-01-2997*, 2004.

[15] R. P. Hessel and C. J. Rutland. A new approach to model DI-diesel HCCI combustion for use in cycle simulation studies. *SAE paper, No. 2005-01-3743*, 2005.

[16] A. Bhave, M. Balthasar, M. Kraft, and F. Mauss. Analysis of a natural gas fuelled homogeneous charge compression ignition engine with exhaust gas recirculation using a stochastic reactor model. *Int. J. Engine Research*, 5(1):93–104, 2004.

[17] H. Su, A. Vikhansky, S. Mosbach, M. Kraft, A. Bhave, F. Mauss, K. O. Kim, and T. Kobayashi. A computational study of an HCCI engine with direct injection during gas exchange. *Combust. Flame*, (1):118–132, 2006.

[18] S. Mosbach, H. Su, M. Kraft, A. Bhave, F. Mauss, Z. Wang, and J. X. Wang. Dual injection HCCI engine simulation using a stochastic reactor model. *Int. J. Engine Research*, 8(1):41–50, 2007.

[19] S. Subramaniam and S. B. Pope. A mixing model for turbulent reactive flows based on euclidean minimum spanning trees. *Combust. Flame*, 115:487–514, 1998.

[20] J.D. Naber and R.D. Reitz. Modeling engine spray/wall impingement. *SAE paper, No. 880107*, 1988.

[21] C. Bai and A. D. Gosman. Development of methodology for spray impingement simulation. *SAE paper, No. 950283*, 1995.

[22] D.W. Stanton and C.J. Rutland. Modeling fuel film formation and wall interaction in diesel engines. *SAE paper, No. 960628*, 1996.

[23] H. Hiroyasu, T. Kadota, and M. Arai. Development and use of a spray combustion modeling to predict Diesel engine efficiency and pollutant emissions (part 1 combustion modeling). *Bulletin of the JSME*, 26(214):569–575, 1983.

[24] J.B. Heywood. *Internal combustion engine fundamentals*. McGRAW-HILL, 1988.

[25] Z. Han, Z. Xu, and N. Trigui. Spray/wall interaction models for multidimensional engine simulation. *Int. J. Engine Research*, 1(1):127–146, 2000.

[26] B. Abramzon and W. A. Sirignano. Droplet vaporization model for spray combustion calculations. *Int. J. Heat Mass Transfer*, 32(9):1605–1618, 1989.

[27] C. A. Chryssakis, D. N. Assanis, S. Kook, and C. Bae. Effect of multiple injections on fuel-air mixing and soot formation in diesel combustion using direct flame visualization and CFD techniques. In *ASME Internal Combustion Engine Division 2005 Spring Technical Conference*, ICES2005-1016, April 5-7, 2005, Chicago, IL, USA, 2005.

6 Appendix

The stochastic reactor model (SRM) can be written as

$$\begin{aligned}
&\tfrac{\partial}{\partial t}\mathcal{F}(\psi,t) + \underbrace{\frac{1}{V}\frac{dV}{dt}\mathcal{F}(\psi,t)}_{\text{piston movement}} + \underbrace{\sum_{i=1}^{s+2}\frac{\partial}{\partial\psi_i}\left[G_i(\psi)\mathcal{F}(\psi,t)\right]}_{\text{chemical kinetics and fuel evaporation}} \\
&+ \underbrace{\frac{1}{h}[U(\psi_{s+1}+h)\mathcal{F}(\psi_1,...,\psi_s,\psi_{s+1}+h,t) - U(\psi_{s+1})\mathcal{F}(\psi,t)]}_{\text{convective heat transfer}} \\
&= \underbrace{\sum_{i=1}^{s+2}\frac{\partial}{\partial\psi_i}\left[A_l(\psi)\mathcal{F}(\psi,t)\right]}_{\text{mixing}} + \underbrace{\frac{{}^{\mathrm{a}}\mathcal{F}_{\mathrm{in}}(\psi,t)}{\tau_{\mathrm{a}}} - \frac{\mathcal{F}(\psi,t)}{\tau_{\mathrm{e}}} + \frac{{}^{\mathrm{f}}\mathcal{F}_{\mathrm{in}}(\psi,t)}{\tau_{\mathrm{f}}}}_{\text{gas exchange and fuel injection}}
\end{aligned} \tag{24}$$

with the initial condition

$$\mathcal{F}(\psi,0) = \mathcal{F}_0(\psi), \tag{25}$$

where $\mathcal{F}$ is the mass density function (MDF), ψ stands for scalar variables such as mass fractions of chemical species and temperature, i.e. $\psi = (\psi_1,...,\psi_s,\psi_{s+1},\psi_{s+2}) = (Y_1,...,Y_s,T,m_d)$. The five terms accounting for piston movement, chemical kinetics and volume change, convective heat transfer, mixing, gas exchange and fuel injection respectively (as indicated in eqn. (24)) are now described in more detail.

The second term on the left hand side (LHS) of eqn. (24) denotes the effect of the piston movement on the MDF. The chemical kinetics and the energy associated with the change in volume is represented by the third term on the LHS where,

$$G_i = \frac{M_i\dot{\omega}_i}{\rho}, \qquad i = 1,\ldots,s, \tag{26}$$

$$G_{s+1} = -\frac{1}{\rho c_{\mathrm{v}}}\sum_{i=1}^{s} e_i M_i\dot{\omega}_i - \frac{p}{mc_{\mathrm{v}}}\frac{dV}{dt}. \tag{27}$$

Here, M_i is the molar mass of species i, ρ is the density of the mixture, $\dot{\omega}_i$ is the molar production rate of the i^{th} species, V is the volume, m is the mass and e_i represents the specific internal energy of species i. In this paper, a deterministic solver based on a backward differentiation formula method was implemented to solve the set of stiff ordinary differential equations.

The fourth term on the LHS of eqn. (24) represents the heat transfer model, where h denotes the fluctuation (the implementation is discussed in section 3.1),

$$U(T) = -\frac{h_g A}{c_{\mathrm{v}} M_{\mathrm{tot}}}(T - T_{\mathrm{W}}), \tag{28}$$

and h_g is the Woschni heat transfer coefficient, A is the heat transfer area, M_{tot} is the total mass, c_{v} is the specific heat capacity at constant volume and T_{W} denotes the wall temperature. Heat transfer occurs between the fluid and the wall due to

convection. It is modelled as a stochastic jump process based on the Woschni heat transfer coefficient [16, 17].

For turbulent mixing $A_l(\psi)$, the EMST model is used [19].

On the RHS of eqn. (24), the last three terms account for the gas exchange and fuel injection processes in a DI HCCI (air intake, exhaust and fuel injection). τ_{a}, τ_{e}, and τ_{f} denote the characteristic residence times of air, exhaust gas and fuel respectively. ${}_{\mathrm{a}}\mathcal{F}_{\mathrm{in}}$, ${}_{\mathrm{f}}\mathcal{F}_{\mathrm{in}}$ stand for mass density function associated with the intake air and fuel streams.